Multilevel Multichannel Study of the Structure of ^{15}N from 12- to 14-MeV Excitation Energy

J. J. Ramirez,* R. A. Blue, and H. R. Weller

Department of Physics, University of Florida, Gainesville, Florida 32601

(Received 9 August 1971)

Measurements of the cross sections for the reactions ^{14}C$(p,p)^{14}$C, ^{14}C$(p,\alpha_0)^{11}$B, ^{14}C$(p,n_0)^{14}$N, ^{14}C$(p,n_1)^{14}$N, ^{14}C$(p,\gamma_0)^{15}$N, and ^{11}B$(\alpha,\alpha)^{11}$B have been made for incident particle energies of 2 to 4 MeV. Preliminary Legendre-polynomial analyses of measured angular distributions were used to guide a multilevel multichannel R-matrix analysis. In the R-matrix formulation a set of level parameters for eight resonances has been found which can account for the observed cross sections in all of the channels. The level at $E_x = 13.42$ MeV in ^{15}N has been identified as the isobaric analog of the second excited state in ^{15}C. The reduced widths of this level in the various channels indicate that it contains at least a 10% admixture of $T = \frac{1}{2}$. A series of strong α-particle levels has been found which fit into the α-particle core-excited threshold-state model scheme for ^{15}N.

I. INTRODUCTION

Previous studies of ^{15}N in the region of excitation energy covered by this work[1-7] have been confined to observations in one channel at a time and, in part due to their limited scope, have yielded few unambiguous results for the level parameters of the structures in ^{15}N. Except for the single-level fits to the ^{14}C$(p,p)^{14}$C cross section below 2.7 MeV,[6,7] no detailed resonance analyses have been performed. Some spin assignments have been suggested[2] on the basis of the behavior of Legendre coefficients obtained in fitting cross sections for the reaction ^{11}B$(\alpha,p)^{14}$C. However, our detailed analysis of all open channels indicates that some of these results are incorrect.

For proton bombardment of ^{14}C below 4 MeV only the proton channels, ground- and first-excited-state α-particle channels, and ground- and first-excited-state neutron channels are open. Our measurements encompass all these particle channels although no α particles leading to the first excited state of ^{11}B were observed. The reaction ^{11}B$(\alpha, \alpha)^{11}$B in the corresponding range of ^{15}N excitation energies was also measured. It was found that the ^{14}C$(p,p)^{14}$C, ^{14}C$(p, \alpha)^{11}$B, and ^{11}B-$(\alpha, \alpha)^{11}$B cross-section data complement each other in that the elastic proton data displayed the strong proton resonances quite clearly, the α elastic data displayed the strong α-particle states most prominently, and the (p, α) data involved both types of states. Without all three measurements, a complete, unambiguous analysis would not have been possible.

The analysis in this work utilized a pure multilevel multichannel R-matrix formalism. The only contributions to the R matrix are those due to

levels explicitly specified with an additional hard-sphere potential scattering term. The complex matrix $(1 - RL_0)$ must be inverted in the process of obtaining the T matrix from which the (p,p), (p, α), (p, n_0), (p, n_1), and (α, α) cross sections were calculated. The region of this experiment included eight levels requiring a large number of parameters. As a result, the complexity of the calculation precluded least-squares fitting of the experimental data. Only a trial-and-error adjustment of the R-matrix parameters was feasible. Preliminary analyses employing Legendre-polynomial fitting and single-level formulations provided the basis for the selection of the trial parameter sets.

The energy region covered in this work includes a number of resonances having particular significance to an understanding of the structure of ^{15}N. An especially strong resonance is observed at $E_p = 3.44$ MeV. This level is assigned a J^π value of $\frac{3}{2}^+$. Since the (p,p) and (p, n_1) processes are the only channels allowing $T = \frac{3}{2}$, a strong resonance in these channels is a good candidate for a $T = \frac{3}{2}$ assignment. In the case of the 3.44-MeV level, however, it is seen that the (p, α) and (p, n_0) channels also display the resonance. This observation is indicative of a strong $T = \frac{1}{2}$ admixture in this $T = \frac{3}{2}$ state.

An examination of the strong α-particle states observed in this region of ^{15}N shows the existence of a $\frac{5}{2}^+, \frac{3}{2}^+, \frac{1}{2}^+$ triplet. This triplet of levels is predicted by the α-particle core-excited threshold-state (APCETS)[8] model. The corresponding $(T = \frac{1}{2})$ triplet in ^{15}O has been identified in previous work.[9] The spacing of these three levels is consistent with an $\vec{I} \cdot \vec{L}$ interaction for the dominant α-particle-core interaction. These states will be discussed extensively in Sec. V.

II. EXPERIMENTAL PROCEDURES

The charged-particle measurements were made in a 56.5-cm-diam scattering chamber with four 300-μm silicon surface-barrier detectors. The ^{14}C targets used for this work were made by cracking 70% ^{14}C-enriched acetylene on a 0.12-μm nickel backing.[10] These targets were approximately 10 keV thick to a 3.4-MeV proton beam. A typical spectrum obtained from proton bombardment of ^{14}C is shown in Fig. 1. The ^{14}C$(p,p)^{14}$C and ^{14}C-$(p, \alpha_0)^{11}$B peaks are clearly resolved. The ^{11}B-$(\alpha, \alpha)^{11}$B measurements were made with a self-supporting target 98% enriched in ^{11}B. The boron target was approximately 25 keV thick for 2.6-MeV α particles. The spectrum obtained for these measurements is shown in Fig. 2.

The absolute cross section for the ^{14}C$(p,p)^{14}$C data was obtained by normalizing to the measurements of Harris and Armstrong[6] at 2.55 MeV. The stated uncertainty in their absolute cross section is ±20%. Since the ^{14}C$(p, \alpha)^{11}$B cross section was measured simultaneously with the elastic cross section, the same normalization factor applies. The absolute cross section for the ^{11}B$(\alpha, \alpha)^{11}$B measurements was determined both by measuring

the target thickness using the energy loss for ^{241}Am α particles and by normalization to the Rutherford cross section at low energy and small scattering angles. The estimated uncertainty in this case is ±20%. The relative uncertainties for the charged-particle cross sections due to statistics are less than 7%.

The neutron measurements were made with a 5×5×2.5-cm NE-102 plastic scintillator coupled to an RCA 8575 photomultiplier tube in a totally enclosed and collimated geometry. The neutrons reaching the detector were collimated by a 2.2-cm-diam aperture in a 92-cm-long paraffin lithium carbonate shield. This detector, used in conjunction with a pulsed proton beam, yielded a time-of-flight spectrum as shown in Fig. 3. An over-all resolving time of 15 nsec, determined primarily by the beam pulse width, was sufficient to resolve the n_0 and n_1 neutron groups from γ rays. The target used for these measurements and the ^{14}C$(p, \gamma_0)^{15}$N measurements was made by cracking 70% ^{14}C-enriched acetylene on a thick tungsten disk. It was determined to be 30-keV thick for 3-MeV protons.

With the neutron detection bias set above 200 keV, the background which underlay the peaks in the time-of-flight spectrum was essentially flat and was easily subtracted without significant error. However, when the detection bias was lowered to 130 keV to permit observation of the n_1 group near threshold the background showed a broad peak indicative of some time correlation to the beam pulse which made reliable background subtraction more difficult. This time-correlated background was apparently due to the detector's response to γ rays produced by neutron absorption in surrounding materials. For background subtraction, spectra were taken with a 25-cm brass shadow bar inserted in the collimator. These spectra closely
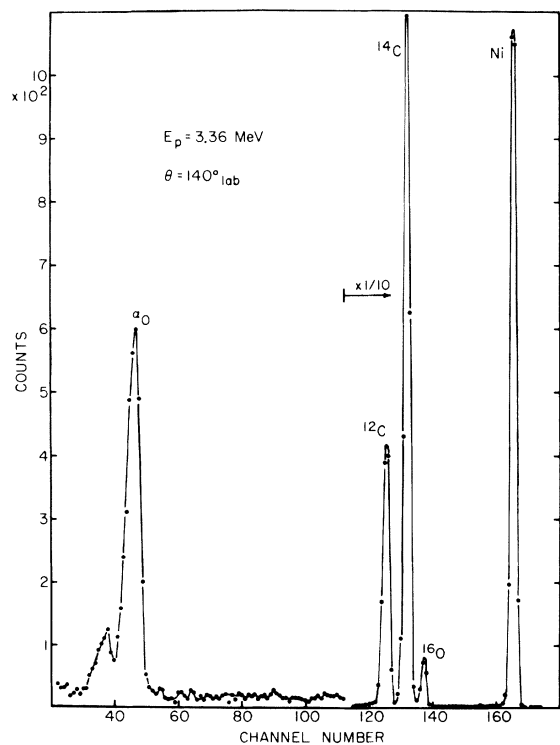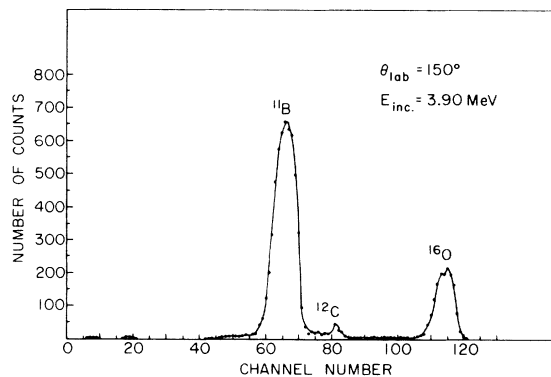

FIG. 1. Charged-particle spectrum from proton bombardment of ^{14}C obtained at a lab angle of 140°. The labeled peaks correspond to elastic scattering from ^{12}C, ^{14}C, ^{16}O, and Ni and to α particles from the reaction ^{14}C$(p, \alpha_0)^{11}$B.

FIG. 2. Charged-particle spectrum from α-particle bombardment of ^{11}B. The elastically scattered α particles from ^{16}O and ^{12}C are also indicated.
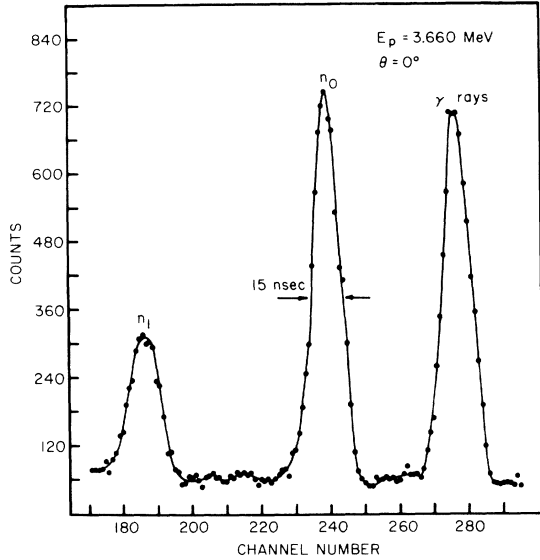
FIG. 3. Time-of-flight spectrum from the reaction ^{14}C-$(p,n)^{14}$N. Time runs from right to left in this figure.

matched the broad background structure when normalized for the same incident total charge. The error in the neutron yield due to this background subtraction is less than 5%.

The relative efficiency of the neutron detector as a function of neutron energy was determined by measuring the yield from the reaction ^{7}Li$(p,n)^{7}$Be and comparing the yield to the known cross section[11] for this reaction. With the neutron detection bias at 130 keV the relative efficiency was found
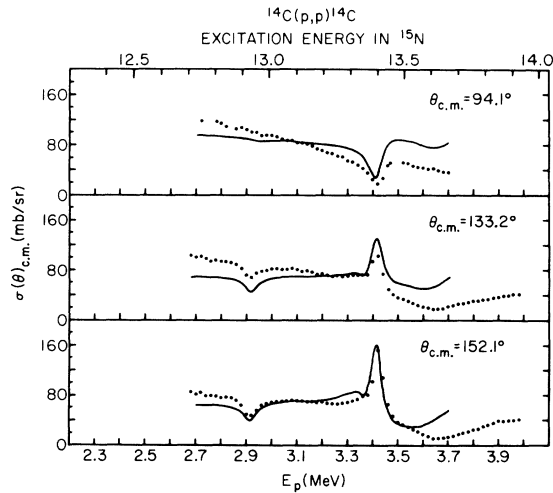
to change rapidly up to about 300 keV. At higher neutron energies the relative efficiency was more nearly constant. After correction for the energy variation of the detection efficiency the neutron yields were normalized to the data of Sanders,[1] who assigned a ±30% uncertainty to his absolute normalization. Statistical uncertainties associated with the present measurements are less than 2% for the n_0 yield and less than 3% for the n_1 yield.

The absolute energy for the ^{14}C$(p,n)^{14}$N measurements was determined relative to the observed ^{7}Li$(p,n)^{7}$Be threshold at 1.881 MeV to an accuracy of ±10 keV. In the case of the reactions ^{14}C$(p,p)^{14}$C and ^{14}C$(p,\alpha_0)^{11}$B the absolute energy scale was fixed by positioning the resonance at 2.49 MeV to coincide with the energy specified by Harris and Armstrong.[6] The estimated energy un-
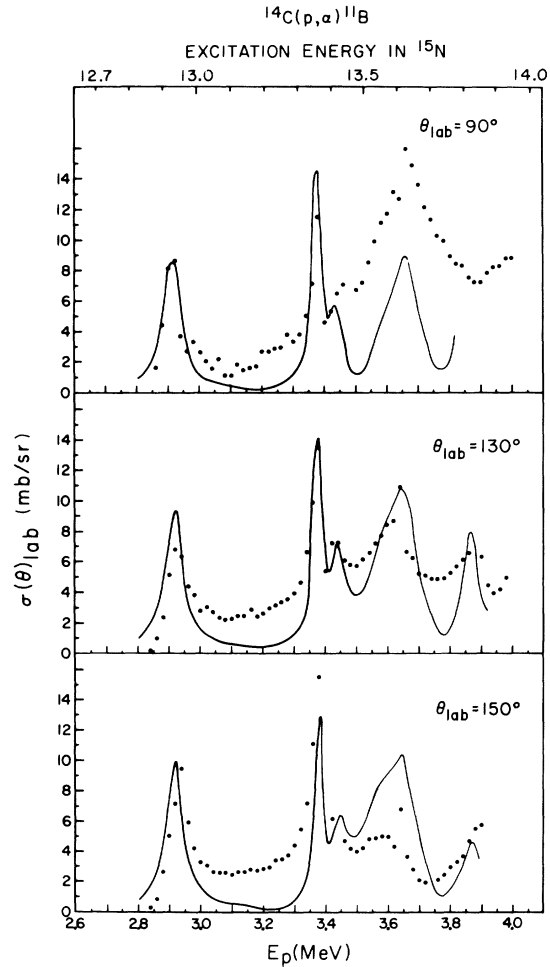

FIG. 4. Excitation curves for the ^{14}C$(p,p)^{14}$C cross section between 2.7 and 4.0 MeV. The solid lines are the result of the R-matrix calculation using the parameters of Table I. The statistical error associated with these data points is less than the size of the dots.

FIG. 5. Excitation curves for the ^{14}C$(p,\alpha)^{11}$B cross section between 2.8 and 4.0 MeV. The solid lines are the result of the R-matrix calculation using the parameters of Table I. The statistical error associated with these data points is less than the size of the dots.

certainty for these measurements is also ±10 keV. Finally, the energy scale for the $^{11}B(\alpha, \alpha)^{11}B$ measurements was adjusted so that the resonance at 2.64 MeV as seen in the reaction $^{11}B(\alpha,p)^{14}C$ obtained at the same time was properly aligned with the resonance observed in the inverse reaction $^{14}C(p, \alpha_0)^{11}B$. In this case the absolute energy uncertainty is estimated at ±30 keV.

III. EXPERIMENTAL RESULTS

Data on five different reactions initiated either by $^{14}C + p$ or $^{11}B + \alpha$ were incorporated in this study of the structure of ^{15}N. Although the primary region of interest is for projectile energies from 2.8 to 4.0 MeV, some measurements were extended down to 2.2 MeV. Only representative samples of the data are displayed in the figures, with solid lines showing the theoretical cross sections obtained from the calculation discussed in Sec. IV. The remaining data consisting of three additional angles for the reactions $^{14}C(p,p)^{14}C$ and $^{14}C(p, \alpha_0)^{11}B$ plus the angular-distribution data can be obtained in tabular form from the authors on request.

Selected excitation curves for the reaction $^{14}C-(p,p)^{14}C$ are shown in Fig. 4. Previous measurements[6,7] of the $^{14}C(p,p)^{14}C$ cross section had extended up to 2.7 MeV. Above this energy two additional levels are evident in these data. The strong

level at 3.44 MeV is interpreted as being the $T = \frac{3}{2}$ analog of the second excited state of ^{15}C. It will be discussed in detail in Sec. IV.

Selected excitation functions for the reaction $^{14}C(p, \alpha)^{11}B$ are presented in Fig. 5. The structure seen in these data at 2.92 MeV has been previously discussed by Lee and Schiffer[2] who observed the inverse reaction $^{11}B(\alpha,p)^{14}C$. One other study of the reaction $^{11}B(\alpha,p)^{14}C$ has also been reported,[4] but no analysis was performed. Our measured angular distributions agree well with those obtained in Refs. 2 and 4. These data were fitted with a series expansion in terms of Legendre polynomials up to and including $P_4(\cos\theta)$ using a least-squares-fitting criteria. The coefficients of this expansion, which were used to guide the R-matrix calculation, are displayed in Fig. 6.

No previous measurements have been reported for the reaction $^{11}B(\alpha, \alpha)^{11}B$. The selected excitation curves are shown in Fig. 7. The structure at 2.63 MeV corresponds to the structure seen at $E_p = 2.92$ MeV in the (p,p), (p, α_0), and (p, n) measurements. The level seen in other channels at $E_p = 3.44$ MeV appears at $E_\alpha = 3.31$ MeV. Structures at 2.65, 3.31, and 3.57 MeV appear to have
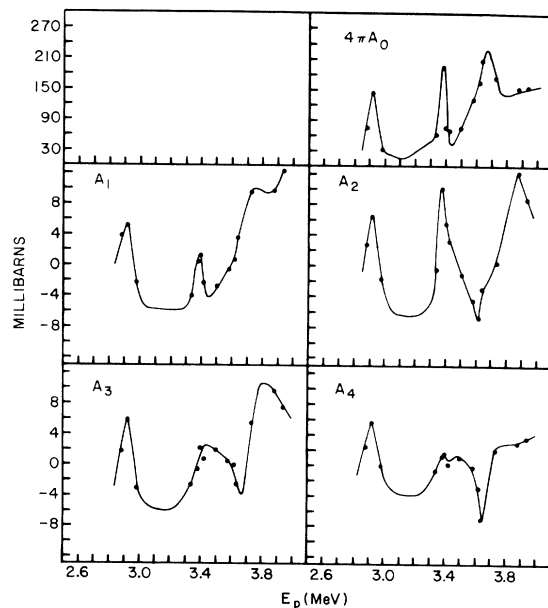

FIG. 6. The Legendre coefficients resulting from fitting the $^{14}C(p, \alpha_0)^{11}B$ angular distributions. The solid lines are smooth curves drawn through the data points. The statistical error associated with the data points is less than the size of the dots.
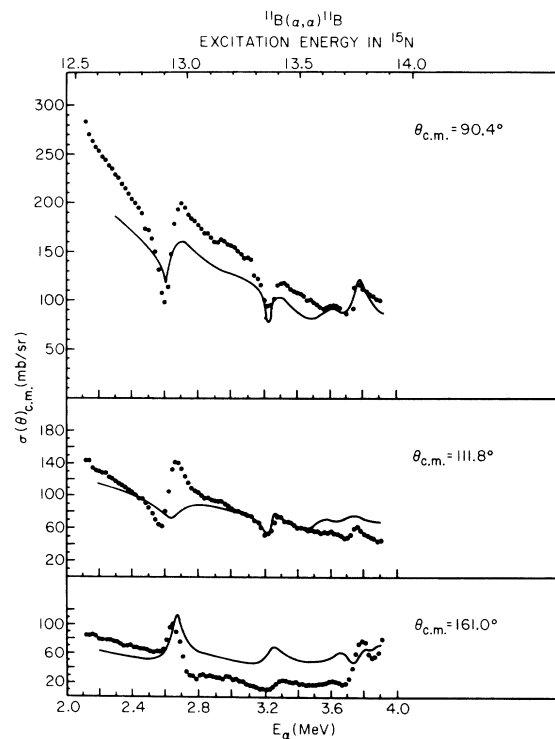

FIG. 7. Excitation curves for the $^{11}B(\alpha, \alpha)^{11}B$ cross section between 2.1 and 3.9 MeV. The solid lines are the result of the R-matrix calculation using the parameters of Table I. The statistical error associated with these data points is less than the size of the dots.

large α widths. These states can be interpreted by the APCETS model, as discussed in Sec. V. Angular-distribution data were obtained for this reaction but are not shown.

Excitation functions for the reaction $^{14}C(p, n_0)^{14}N$ at 0 and 90° are shown in Fig. 8. The 2.92- and the 3.44-MeV structures are seen prominently. Previous measurements have been reported by Sanders[1] and Blair, Edge, and Willard,[3] although no angular-distribution measurements have been reported in this region. In the present work the levels at 3.38 and 3.44 MeV are not resolved because of the 30-keV target thickness, although the weaker 3.38-MeV resonance is clearly responsible for the shoulder on the 3.44-MeV peak. The angular-distribution data obtained in the present work were fitted with a series expansion in terms of Legendre polynomials. The coefficients resulting from these fits are presented in Fig. 9 and will be discussed later regarding their implications on spins and parities.

In most of the previous work, a long counter was employed for neutron detection such that measurements above the n_1 threshold at 3.15 MeV involved the sum of the n_0 and n_1 neutron groups. Very little data have been previously reported for
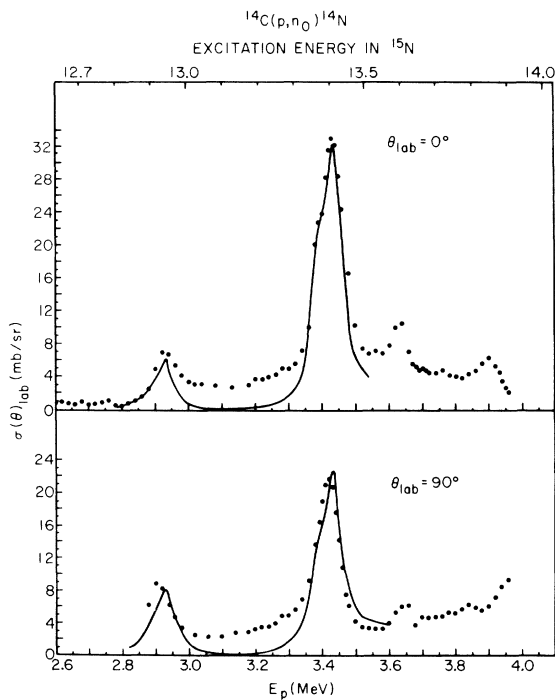
the reaction $^{14}C(p, n_1)^{14}N$.[3] Since the first excited state of ^{14}N is $T = 1$, observations of the n_1 group have a particular significance in the discussion of the $T = \frac{3}{2}$ state at $E_p = 3.44$ MeV. Our measured excitation curve for $^{14}C(p, n_1)^{14}N$ at 0° is shown in Fig. 10. Angular distributions were fitted with a series expansion in terms of Legendre polynomials. The coefficients obtained are shown in Fig. 11.

In addition to the reactions mentioned above, the reaction $^{14}C(p, \gamma_0)^{15}N$ was studied in the vicinity of the 3.44-MeV resonance. As would be expected for a $T = \frac{3}{2}$ state, a strong resonance was observed. These results will be presented in conjunction with the discussion of the structure of the $T = \frac{3}{2}$ state at 3.44 MeV in Sec. V.

IV. MULTILEVEL MULTICHANNEL R-MATRIX ANALYSIS

The computer code MULTI[12] was used for the R-matrix analysis of these data. This code employs the formalism of Lane and Thomas[13] with the R

FIG. 8. Excitation curves for the $^{14}C(p, n_0)^{14}N$ cross section between 2.6 and 3.9 MeV. The solid lines are the result of the R-matrix calculation using the parameters of Table I. The statistical error associated with these data points is less than the size of the dots.
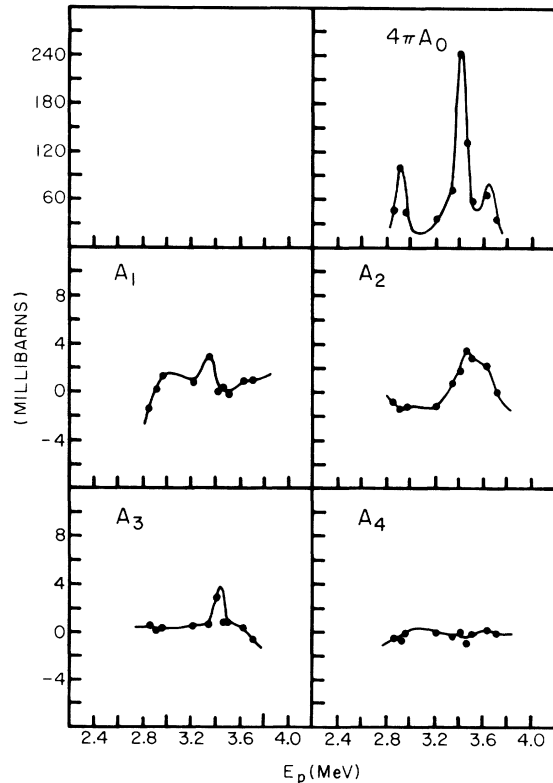

FIG. 9. The Legendre coefficients resulting from fitting the $^{14}C(p, n_0)^{14}N$ angular distributions. The solid lines are smooth curves drawn through the data points. The statistical error associated with these data points is less than the size of the dots.

matrix defined as

$$R_{cc'} = \sum_\lambda \frac{\gamma_{\lambda c}\gamma_{\lambda c'}}{E_\lambda - E}.$$

The sum is over the levels of the compound system labeled by λ. The contribution of each level is determined by the resonance energy, E_λ, and the reduced widths in each channel, $\gamma_{\lambda c}^2$. Given R, the scattering matrix U is found from

$$U = \Omega P^{1/2}(1 - RL_0)^{-1}(1 - RL_0^*)P^{-1/2}\Omega.$$

As indicated, the complex matrix $(1 - RL_0)$ must be inverted. Next, the T matrix is obtained from

$$T_{cc'} = e^{2i\omega\alpha'l'}\delta_{\alpha's'l'; \alpha sl} - U^{J\pi}_{\alpha's'l'; \alpha sl}.$$

The undefined quantities in these expressions appear in Lane and Thomas.[13] The cross section in each channel can be computed directly from T.

The nonresonant phase shifts are taken to be Coulomb plus hard sphere in this calculation. No background was included, so that only the levels explicitly specified contribute to the reaction cross section. The boundary-condition parameter was set equal to the shift function at the midpoint energy of the calculation. In addition, the value of R_0 (the constant which determines the channel radii) was taken to be 1.45 fm. The program in its present form allows for 20 levels, 35 channels, 7

different J^π values and values of $l \leqslant 4$. A Gaussian smear is also included to account for the finite target thicknesses. This smear width was taken to be 10 keV for the protons, 20 keV for the α particles, and 30 keV for the neutrons, in accord with the measured target thicknesses.

In the next section we will discuss results derived from fitting the various resonance structures observed in this experiment. It was found that the many levels and channels are sensitively coupled. Although much better agreement between the calculated and observed cross sections could have been obtained for any given reaction, consideration of all the available data provides severe constraints on the parameters used in calculating the cross sections. The basic procedure employed began with Legendre-polynomial fits to angular distributions for each of the reaction channels. These results next guided single-level fits to each resonance. The level parameters in a multilevel calculation were then slowly varied to obtain a consistent set of parameters which could simultaneously fit all the data with all levels and
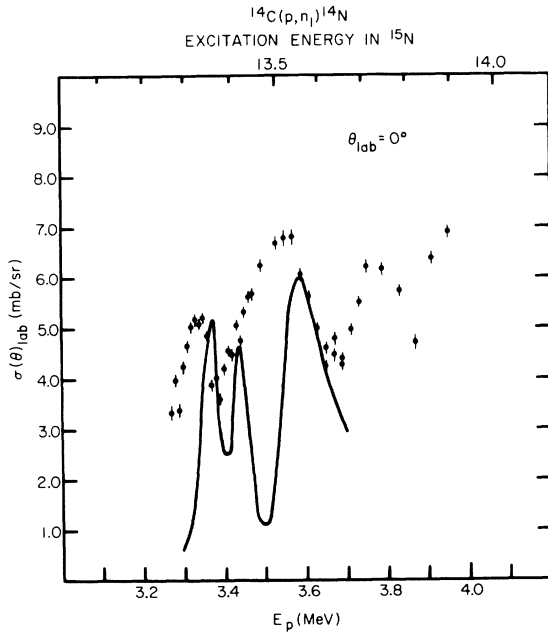
FIG. 10. Excitation curve for the $^{14}C(p,n_1)^{14}N$ cross section between 3.3 and 4.0 MeV. The solid line is the result of the R-matrix calculation using the parameters of Table I. The error bars represent the statistical error associated with the data points.
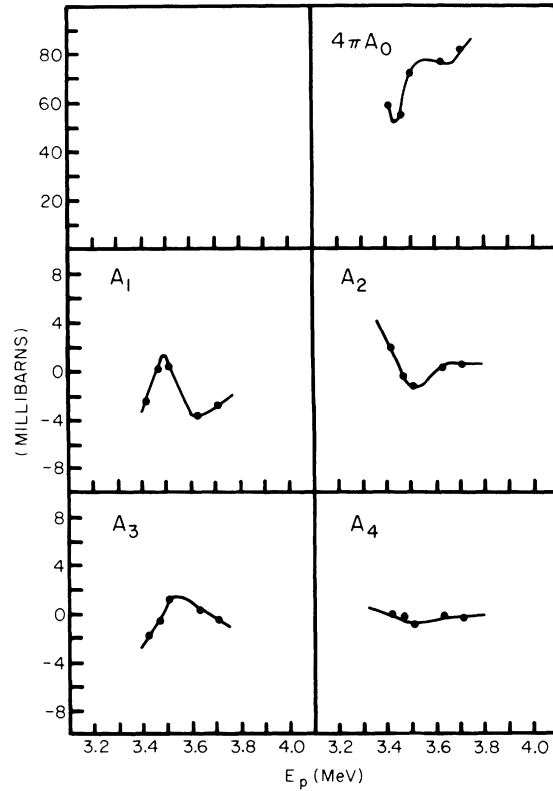
FIG. 11. The Legendre coefficients resulting from the fits to the $^{14}C(p,n_1)^{14}N$ angular distributions. The solid lines are smooth curves drawn through the data points. The statistical error associated with these data points is less than the size of the dots.

channels included. The large number of parameters and the complexity of the multilevel multichannel calculations made any form of automatic parameter searching impractical. Although this procedure is quite cumbersome, an analysis of this complexity is required to obtain unambiguous results. So, for example, simultaneous fitting of (p,p), (p,α), and (α,α) data on the same level allowed a unique fit where the results would be obscured if part of the data were lacking.

$\frac{3}{2}^-, \frac{5}{2}^+$ Doublet at $E_x = 12.93$ and 12.94 MeV

Even though the structure seen in the cross section may appear to involve a single level, closer examination reveals that it is in fact a doublet. This doublet has previously been discussed by Lee and Schiffer,[2] who studied the reaction $^{11}B(\alpha,p)^{14}C$. They assigned spin parities of $\frac{3}{2}^-, \frac{7}{2}^-$ on the basis of the behavior of the coefficients of Legendre polynomials obtained from angular distributions. In their analysis, however, they assumed that only a single l value contributed for each level of a given J^π, an assumption which cannot be justified. Furthermore, it was claimed that the coefficients of the P_1 and P_3 terms do not resonate, indicating that the levels are of the same parity. This latter statement is the result of the unfortunate practice of presenting the coefficients as the ratio A_n/A_0 rather than the coefficients of the Legendre polynomials themselves. In the work of Ref. 4 as well as in the results of our measurements (see Fig. 6), we see that A_1 and A_3 do in fact resonate, indicating that P_1 and P_3 make substantial contributions in this energy region. We therefore conclude that the two states must be of opposite parity. It is also found that P_4 is the highest-order polynomial needed. This result indicates, from the properties of the $\overline{Z}$ coefficients,[14] that the doublet involves levels having spin parities of $\frac{1}{2}^-$ or $\frac{3}{2}^-$ and $\frac{3}{2}^+$ or $\frac{5}{2}^+$, respectively. In examining the other channels we first note in Fig. 4 that the (p,p) cross section does not show resonance structure at 90°. This suggests that the negative-parity state dominates this channel. The Legendre coefficients for the n_0 channel (see Fig. 9) do not have significant values for the odd terms, but A_0 and A_2 are present. This suggests, from the properties of the $\overline{Z}$ coefficients,[14] that only the odd-parity state is important for this channel also. Finally, it is clear from Fig. 7 that the $^{11}B(\alpha,\alpha)^{11}B$ channel also shows this doublet at $E_\alpha = 2.65$ MeV.

Having seen that resonance behavior due to this doublet is observed in the reactions $^{11}B(\alpha,\alpha)^{11}B$, $^{14}C(p,p)^{14}C$, $^{14}C(p,n_0)^{14}N$, and $^{14}C(p,\alpha)^{11}B$, with the restrictions on spin parities as discussed in the previous paragraph in mind, we began a mul-

tilevel multichannel calculation for this region. Our first results indicated that the negative-parity level had to be $\frac{3}{2}^-$ to reproduce the forward-angle dip in the $^{11}B(\alpha,\alpha)^{11}B$ data (see Fig. 7). This assignment is consistent with the measurements of Lee and Schiffer,[2] and can well account for the (p,p) and (p,n_0) data in Figs. 4 and 8.

The remaining ambiguity involves the assignment for the positive-parity member of the doublet. It was found that the backward-angle behavior of the $^{11}B(\alpha,\alpha)^{11}B$ data could only be obtained with a $\frac{5}{2}^+$ or $\frac{3}{2}^+$ assignment as previously expected, but these data gave no clear basis for distinguishing between these two possible assignments. The previous $\frac{7}{2}^-$ assignment for this level proved to be completely incapable of reproducing the observed shapes in this cross section. The $^{14}C(p,\alpha_0)^{11}B$ angular distribution, however, proved to be sensitive to the $\frac{3}{2}^+, \frac{5}{2}^+$ assignment. In Fig. 12 we display the fit obtained for the $\frac{5}{2}^+$ assignment for the second member of the doublet. This fit is significantly better than any which could be obtained with a $\frac{3}{2}^+$ assignment. On the basis of the analysis of all of the available data, the $(\frac{3}{2}^-, \frac{5}{2}^+)$ assignment has been well substantiated for this doublet.

In analyzing the angular distribution at $E_p = 2.92$ MeV for the (p,n_0) reaction we found that a pure $l=1$ decay best fit the data. It is interesting to note the values of the relative widths for $l=1$ decay among the allowed channels corresponding to channel spins of $\frac{1}{2}$ and $\frac{3}{2}$. The shape of the angular distribution is very sensitive to the values of these parameters (see Table I) so they are quite uniquely
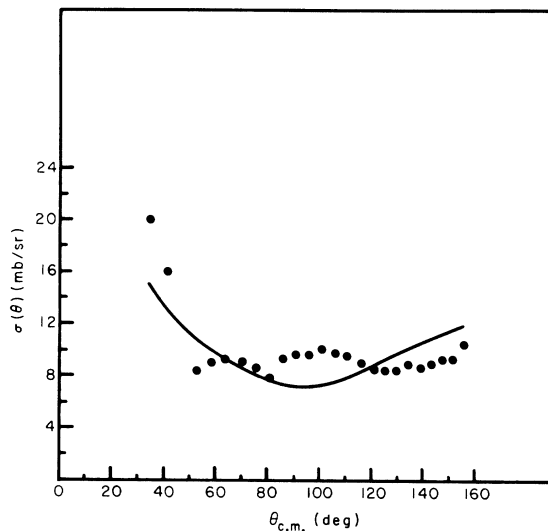
FIG. 12. The measured and theoretical angular distribution for the reaction $^{14}C(p,\alpha_0)^{11}B$ at 2.92 MeV. The statistical error associated with the data points is less than the size of the dots.

determined. The resulting fit to the (p, n_0) angular distribution is shown in Fig. 13.

It must be mentioned that all of the fits displayed result from the full multilevel multichannel calculation including all the levels as specified in Table I. In practice, of course, an iterative procedure was employed; and a consistent set of parameters was ultimately obtained, although initially each resonance was investigated as an isolated structure. The final calculations of excitation curves for this doublet are shown in Figs. 4, 5, 7, and 8.

$\frac{3}{2}^-$ Level at $E_x = 13.36$ MeV

This level is observed in all of the investigated channels. Lee and Schiffer[2] have given a $\frac{3}{2}^-$ assignment to this level based on the Legendre-polynomial behavior obtained from the $^{11}B(\alpha, p)^{14}C$ cross section and the value of the cross section at the peak of the resonance. Our multilevel multichannel analysis confirms this assignment. We found that only the $\frac{3}{2}^-$ assignment could reproduce the value of the cross sections at the peak of the resonance. This is the first level seen in the (p, n_1) channel. The parameters for the n_1 channel, however, must be taken cautiously because of the small amount of data obtained in this case.

Other parameters for the level are quite well determined, as, for example, the distribution of strength between the two l values in the α channel (see Table I). This particular distribution is required in order to reproduce the shape of the (p, α) and (α, α) cross sections. The strength in the proton channel determines the strength in all other (p, x) channels. Thus, requiring a fit to (p, p), (p, α), (p, n), and (α, α) cross sections de-
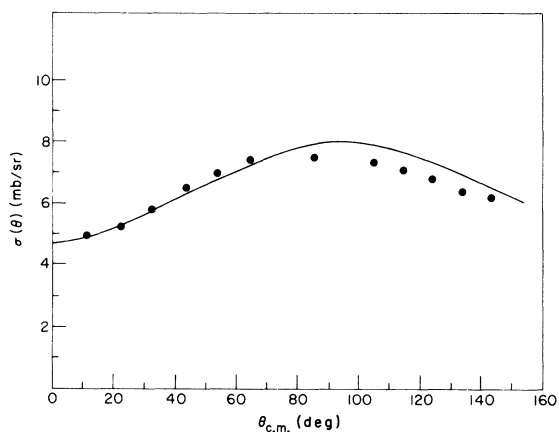

FIG. 13. The measured and theoretical angular distribution for the reaction $^{14}C(p, n_0)^{14}N$ at 2.92 MeV. The statistical error associated with the data points is less than the size of the dots.

fines a quite unique value for the width in each channel.

$\frac{3}{2}^+$ Level at $E_x = 13.42$ MeV

The level at $E_x = 13.42$ MeV corresponding to $E_p = 3.44$ MeV shows up very strongly in the proton channel.[15] A single-level analysis of these data indicated that the behavior of the (p, p) cross section at this energy could be accounted for by a $\frac{3}{2}^+$ or $\frac{5}{2}^+$ spin assignment, with the $\frac{3}{2}^+$ giving a better fit to the peak of the resonance as a function of angle.[15] A multilevel multichannel analysis (eventually including seven adjacent levels) indicated that a set of parameters which simultaneously fit all channels could be found. A critical test of the spin assignment was the n_0 angular distribution on this resonance. This can be well accounted for by $l = 0$ decay only. This l value is allowed for $\frac{3}{2}^+$, but is prohibited for a $\frac{5}{2}^+$ assignment. The resulting fit to the (p, n_0) angular distribution is shown in Fig. 14. The fits to the (p, α_0) angular distributions in this energy region are also shown here. Since our initial report of this level [which we assigned $J^\pi(T) = \frac{3}{2}^+ (\frac{3}{2})$], Kuan[16] has independently assigned $J^\pi = \frac{3}{2}^+$ from the measured γ-ray angular distribution. Further support for this assignment comes from a Nilsson-model calculation[17] which suggests $\frac{3}{2}^+ (\frac{3}{2})$. This calculation and other properties of this level will be discussed in Sec. V. The earlier assignment[2] of $\frac{5}{2}^+$ is clearly incorrect. At first, the fact that this state decays more strongly through the n_0 channel $(T = \frac{1}{2})$ than it does through its n_1 channel $(T = \frac{1}{2}$ or $\frac{3}{2})$ may seem surprising. This is, however, easily attributable to the differences in penetrabilities, as can be seen by comparison of the reduced widths for these channels given in Table I.

$\frac{3}{2}^-$ Level at $E_x = 13.54$ MeV

This level was introduced primarily on the basis of observations in the n_1 channel (see Fig. 10). Lee and Schiffer[2] have previously argued for a broad $\frac{3}{2}^-$ level in this energy region. The behavior of the Legendre coefficients for the n_1 channel indicate that P_0 and P_2 terms are required, while the coefficient of P_4 is essentially zero in this region ($E_p = 3.57$ MeV). This result indicates a $\frac{1}{2}^-$ or $\frac{3}{2}^-$ assignment. The fact that the coefficients of P_1 and P_3 are rapidly changing in this region suggests interference with states of opposite parity. It was found that with this $\frac{3}{2}^-$ level included, the (p, α_0) cross section dropped lower between the two levels at $E_p = 3.38$ and 3.44 MeV and gave a larger separation of the resonance peaks as is observed in the backward-angle data of this channel. The inclusion of this level is also crucial for the

TABLE I. The set of resonance parameters used to obtain the fits to the cross-section data of this experiment. The parameters for the last two levels are somewhat questionable, since not all the channels were fitted in this region.

E_p (lab) (MeV)	E_α (lab) (MeV)	E_x (MeV)	J^π	$\Gamma_{c.m.}$ (keV)	S	l	Partial width (keV)	Reduced width (keV)
2.91	2.64	12.93	$\frac{3}{2}^-$	69.0	$\frac{1}{2}$	1	$\Gamma_p=9.0$	5.78
					$\frac{3}{2}$	0	$\Gamma_\alpha=15.0$	11.36
					$\frac{3}{2}$	2	$\Gamma_\alpha=20.0$	57.07
					$\frac{1}{2}$	1	$\Gamma_{n_0}=7.0$	3.29
					$\frac{3}{2}$	1	$\Gamma_{n_0}=18.0$	8.45
					$\frac{3}{2}$	3	$\Gamma_{n_0}=0.0$	0
2.93	2.66	12.94	$\frac{5}{2}^+$	80.5	$\frac{1}{2}$	2	$\Gamma_p=0.5$	0.97
					$\frac{3}{2}$	1	$\Gamma_\alpha=40.0$	44.75
					$\frac{3}{2}$	3	$\Gamma_\alpha=40.0$	437.00
					$\frac{1}{2}$	2	$\Gamma_{n_0}=0.0$	0
					$\frac{3}{2}$	2	$\Gamma_{n_0}=0.0$	0
					$\frac{3}{2}$	4	$\Gamma_{n_0}=0.0$	0
3.38	3.23	13.36	$\frac{3}{2}^-$	25.6	$\frac{1}{2}$	1	$\Gamma_p=6.3$	3.33
					$\frac{3}{2}$	0	$\Gamma_\alpha=8.5$	3.73
					$\frac{3}{2}$	2	$\Gamma_\alpha=3.5$	3.98
					$\frac{1}{2}$	1	$\Gamma_{n_0}=2.0$	0.81
					$\frac{3}{2}$	1	$\Gamma_{n_0}=2.0$	0.81
					$\frac{3}{2}$	3	$\Gamma_{n_0}=2.0$	11.46
					$\frac{1}{2}$	1	$\Gamma_{n_1}=1.3$	6.98
3.44	3.31	13.42	$\frac{3}{2}^+$	61.1	$\frac{1}{2}$	2	$\Gamma_p=35.0$	46.53
					$\frac{3}{2}$	1	$\Gamma_\alpha=0.0$	0
					$\frac{3}{2}$	3	$\Gamma_\alpha=5.5$	18.10
					$\frac{3}{2}$	0	$\Gamma_{n_0}=19.0$	5.62
					$\frac{1}{2}$	2	$\Gamma_{n_1}=1.6$	170.8
3.57	3.47	13.54	$\frac{3}{2}^-$	133.0	$\frac{1}{2}$	1	$\Gamma_p=8.0$	3.94
					$\frac{3}{2}$	0	$\Gamma_\alpha=25.0$	9.44
					$\frac{3}{2}$	2	$\Gamma_\alpha=20.0$	17.76
					$\frac{1}{2}$	1	$\Gamma_{n_0}=20.0$	7.70
					$\frac{3}{2}$	1	$\Gamma_{n_0}=20.0$	7.70
					$\frac{1}{2}$	1	$\Gamma_{n_1}=40.0$	100.2
3.65	3.57	13.61	$\frac{1}{2}^+$	94.0	$\frac{1}{2}$	0	$\Gamma_p=12.0$	4.13
					$\frac{3}{2}$	1	$\Gamma_\alpha=62.0$	28.78
					$\frac{1}{2}$	0	$\Gamma_{n_0}=20.0$	5.70
3.81	3.78	13.76	$\frac{1}{2}^+$	69.5	$\frac{1}{2}$	0	$\Gamma_p=0.5$	0.17
					$\frac{3}{2}$	1	$\Gamma_\alpha=69.0$	27.7
3.87	3.86	13.82	$\frac{3}{2}^+$	40.0	$\frac{1}{2}$	2	$\Gamma_p=30.0$	30.9
					$\frac{3}{2}$	1	$\Gamma_\alpha=5.0$	1.9
					$\frac{3}{2}$	3	$\Gamma_\alpha=5.0$	8.1

(α, α) reaction. Improved fits in all channels
were obtained with this assignment. However,
since this level is primarily observed through its
effects on other levels and the background, this
assignment cannot be regarded as being definitive.

13.64-, 13.76-, and 13.82-MeV Levels

Assignments for these last three levels came
primarily from the (α, α) data. These levels are
predominantly α-particle levels and so are only
seen in the (p, α) and the (α, α) reactions. The
fits to the (α, α) channel are quite good at the for-
ward angles, but in the backward angles where
the potential scattering becomes more important,
the off-resonance cross section is not reproduced.
This is probably due to the neglect of levels which
are strong in other channels. Since the strength
of a level is well determined by the spin for the
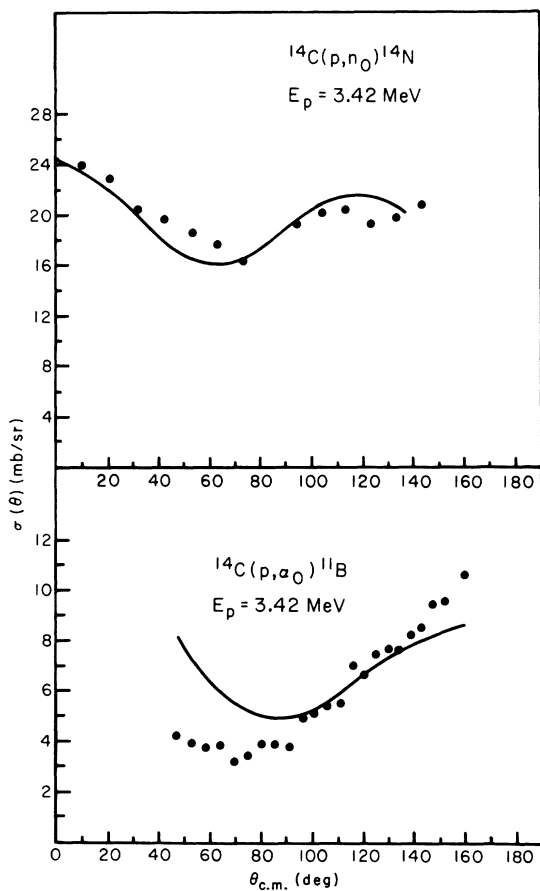case where decay occurs primarily through one

channel, there is little ambiguity in making these
spin assignments. The inclusion of these levels
in the (p, α) calculation improves the fits although
it is clear that some background, presumably due
to neglected levels, is missing. Due to this ne-
glect, the resonance parameters for these levels
must be regarded with caution. Further support
for these assignments comes from the APCETS
model[8] and will be discussed in the following sec-
tion.

V. DISCUSSION OF RESULTS

The most striking feature of the elastic proton
data is the strong resonance at $E_p = 3.44$ MeV (lab).
This level (assigned a J^π of $\frac{3}{2}^+$) is, by virtue of its
large proton reduced width (see Table I), a good
candidate for a $T = \frac{3}{2}$ state. Further experimental
evidence for this comes from measurements of
the reaction $^{14}C(p, \gamma)^{15}N$. Contrary to our previous
report[15] this level decays primarily to the ground
state of ^{15}N. This result was first obtained by
Kuan,[16] who reported that the level decays 93% to
ground and 7% to the 5.30, 5.27-MeV doublet of
^{15}N. An angular-distribution measurement of the
γ rays to ground confirms our $\frac{3}{2}^+$ assignment. Fig-
ure 15 shows the $^{14}C(p, \gamma_0)^{15}N$ ground-state yield
which we obtained with a 12.7×12.7-cm NaI crys-
tal positioned at 60° with respect to the beam at a

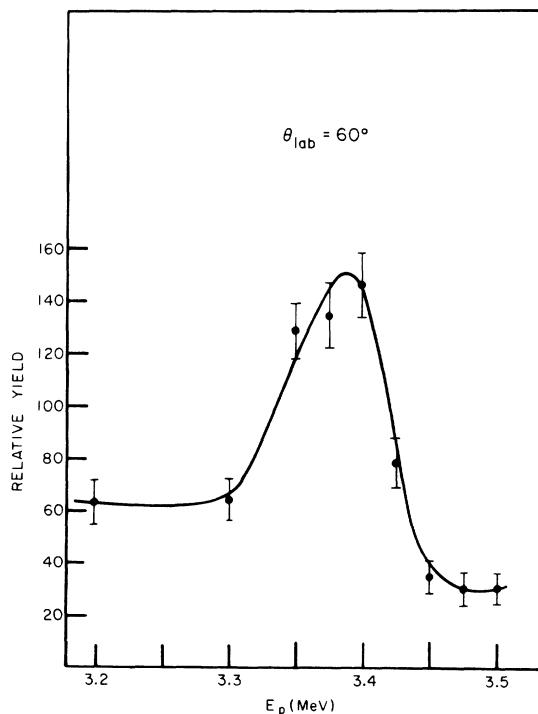FIG. 14. The measured and theoretical angular distri-
butions for the reactions $^{14}C(p, n_0)^{14}N$ and $^{14}C(p, \alpha_0)^{11}B$
at 3.42 MeV. The statistical error associated with the
data points is less than the size of the dots, unless other-
wise indicated.

FIG. 15. The measured excitation curve for the reac-
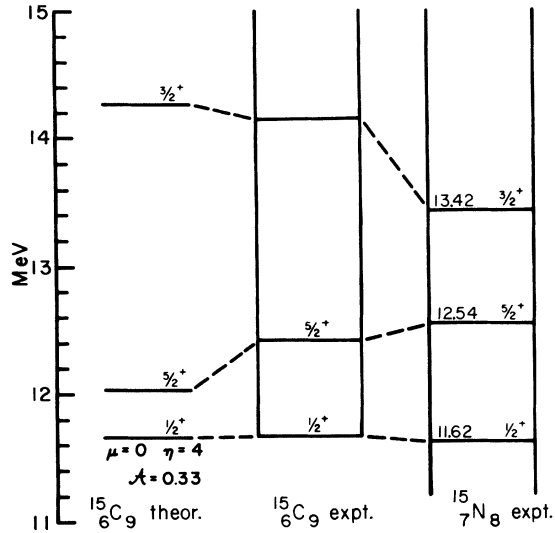tion $^{14}C(p, \gamma_0)^{15}N$ in the vicinity of the 13.42-MeV level.

FIG. 16. Energy-level diagram of the observed states in ^{15}C and ^{15}N. Only $T=\frac{3}{2}$ states in ^{15}N are shown. Also shown are the theoretical levels of ^{15}C from the Nilsson-model calculation of Bhatt (Ref. 17). Both the electrostatic energy difference (Ref. 18) and the neutron-proton mass difference have been removed.

distance of 6.4 cm from the target. Besides the proton and γ-ray channels, we have seen that this level occurs in the n_0, n_1, and α channels. The fits obtained are based on the assumption that one level is responsible for all the channels. This result implies that the isospin of the level is not pure, since the n_0 and α channels are $T=\frac{1}{2}$ channels.

A measure of the isospin impurity of this level can be obtained by computing the quantity

$$R = \frac{\gamma_{n_1}^2 + \gamma_p^2}{\gamma_{n_1}^2 + \gamma_p^2 + \gamma_{n_0}^2 + \gamma_\alpha^2} = 0.90 .$$

This is the ratio of the $T=\frac{3}{2}$ allowed reduced widths to the sum of all reduced widths for this level. Hence we see that there is at least a 10% $T=\frac{1}{2}$ admixture in this level. Of course, this number gives an estimate only of the minimum isospin admixture, since the p and n_1 channels can also decay via $T=\frac{1}{2}$. The value of $\gamma_{n_1}^2$ is crucial in determining the value of R. The small amount of data in the n_1 channel resulted in a rather uncertain value for $\gamma_{n_1}^2$. However, in order to assure that we obtained a valid minimum value for the mixing, we attempted to maximize $\gamma_{n_1}^2$ in fitting the data.

In performing this analysis we assumed that there was a single level of mixed isospin which is responsible for the resonance observed with various channels. The alternative is to assume that there are two levels at the same energy having about the same widths, spins, and parities, but different isospins. The success of our calculations in which the full width of a single level was exhausted when distributed among the various open channels supports our assumption of a single level of mixed isospin. However, the complexity of the multilevel multichannel calculation is such that this result is not completely definitive. Theoretically, both a pure $T=\frac{3}{2}$ ($\frac{3}{2}^+$) state and a pure $T=\frac{1}{2}$ ($\frac{3}{2}^+$) state in this energy region can be described by quite simple models, a Nilsson model and an α-cluster model, respectively.

The energy-level diagram for the known $T=\frac{3}{2}$ states in ^{15}N and their analogs in ^{15}C is shown in Fig. 16. The electrostatic energy difference and the neutron-proton mass difference[18] have been removed. We have assumed that the level at 2.48 MeV in ^{15}C is a $\frac{3}{2}^+$ state. This is supported by the Nilsson-model calculations for nine-neutron nuclei by Bhatt.[17] In this work, the extreme single-particle model is assumed, the bands available to the last odd particle are mixed, and the energy
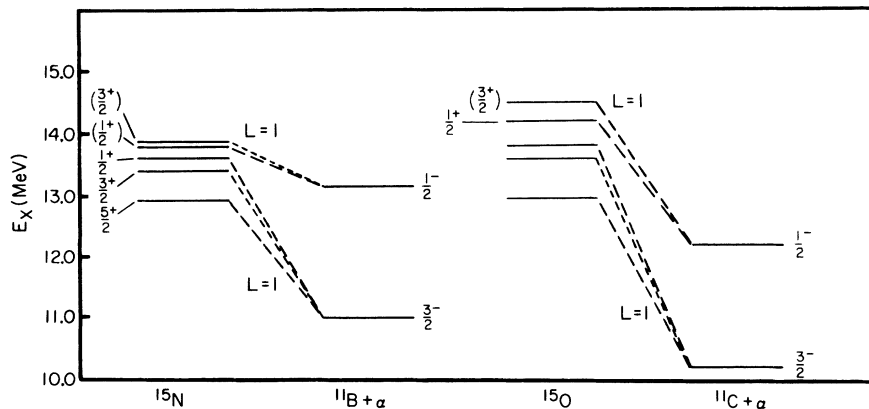

FIG. 17. The known α-particle levels in the 12-15-MeV region of ^{15}O and ^{15}N are shown. Also indicated are the core states which yield the observed multiplets when coupled to $L=1$ α particles, as predicted by the APCETS model (Ref. 8).

matrices are diagonalized to obtain the spectra and the wave functions. The parameters μ, η, and A are defined in Ref. 17. The calculated spectrum of Fig. 16 is for $\mu = 0$, $\eta = 4$, and $A = 0.33$. We see that the position of the $\frac{3}{2}^{+}$ state suggests that the second excited state of ^{15}C has J^{π} of $\frac{3}{2}^{+}$. However, a direct measurement of this J^{π} value is needed before a positive identification can be made.

Previous studies[8,19,20] of ^{15}O have indicated the existence of a series of levels in ^{15}O built of a ^{11}C excited core coupled to an α particle with the ground-state system being near the binding energy of an α particle in ^{15}O (the APCETS model). Further studies have shown that the relative orbital angular momentum between the α particle and the core is $L = 1$. This results in a series of multiplets. The doublet corresponding to the coupling of the $\frac{1}{2}^{-}$ first excited state to an $L = 1$ α particle has been identified in a study of the reaction ^{12}C-$(^{3}\text{He}, \alpha)^{11}$C.[20] The triplet built on the ground state cannot be seen with the reaction used for the higher states, but a triplet of levels has been observed via the reaction ^{14}N$(p, \alpha)^{11}$C.[9] In Fig. 17 we show these five levels of ^{15}O. The five levels in ^{15}N having positive parity as obtained in this experiment are also shown. We see that the spins of the lowest three levels are as expected from the APCETS model. Furthermore, the spacings of the $(\frac{5}{2}^{+}, \frac{3}{2}^{+}, \frac{1}{2}^{+})$ levels tend to agree with what is expected if the interaction responsible for the splitting of the multiplet is primarily of the $\vec{I} \cdot \vec{L}$ form. Namely, the spacing goes as the ratio of the spins of the lower levels (5 : 3 here). Credible spin assignments for the corresponding three levels in ^{15}O are still lacking. It is, however, encouraging to note that the relative spacings are similar to the ^{15}N case.

At this point we have both a single-particle $(T = \frac{3}{2})$ and an α-particle $(T = \frac{1}{2})$ description for the isospin-mixed $\frac{3}{2}^{+}$ state in ^{15}N. A unified description of this state remains to be formulated.

In the energy range between 13–14 MeV the structure of ^{15}N is dominated by a series of strong positive-parity states having relative simple descriptions. The other states observed in this work are all $\frac{3}{2}^{-}$. In a discussion of the $\frac{3}{2}^{-}$ third excited state of ^{15}N, Lopes et al.[21] assert that the

unperturbed $(1p_{3/2})^{-1}$ hole state should lie in the 8–10-MeV energy region relative to the ^{15}N ground state. This $\frac{3}{2}^{-}$ strength is apparently spread through the energy region covered by the present work. It is reasonable to assume that the energy range 13–14 MeV includes states other than those we have discussed. The observed cross sections give slight indications of a number of weaker resonances. The existence of levels which we have not included in our analysis probably accounts for much of the discrepancy between calculated and observed cross sections, particularly in the regions between the strong resonances.

SUMMARY

We have seen that a complete measurement of all open channels can result in a unique parametrization of data in a complex situation. It is obvious to us that a reliable R-matrix analysis can only begin to be made when all the channels are experimentally determined. As the energy is raised, more levels and channels appear, and the increasing complexity makes this type of analysis completely untenable. In a continuation of this work we have extended the ^{11}B$(\alpha, \alpha)^{11}$B measurements to $E_{\alpha} = 8$ MeV. At these energies it appears more promising to use a complex potential to account for the multichannel nature of the problem. In this case, the background (off-resonance) cross section cannot be reproduced if hard-sphere potential scattering is used.

The present work has shown that the region of ^{15}N between 13 and 14 MeV displays a number of remarkably simple structures including $T = \frac{3}{2}$ states and α-particle states well described by the APCETS model. It is clear that high excitation energies are not completely synonymous with complicated wave functions or a statistical-nucleus situation.

ACKNOWLEDGMENTS

*Present address: Western Michigan University, Kalamazoo, Michigan 49001.

[1]R. W. Sanders, Phys. Rev. 104, 1434 (1956).

[2]L. L. Lee and J. P. Schiffer, Phys. Rev. 115, 160 (1959).

[3]J. K. Bair, R. D. Edge, and H. B. Willard, Phys. Rev. 119, 1948 (1960).

[4]G. S. Mani, P. D. Forsyth, and R. R. Perry, Nucl. Phys. 44, 625 (1963).

[5]G. S. Mani and G. C. Dutt, Nucl. Phys. 78, 613 (1966).

[6]W. R. Harris and J. C. Armstrong, Phys. Rev. 171, 1230 (1968).

[7]J. D. Henderson, E. L. Hudspeth, and W. R. Smith, Phys. Rev. 172, 1058 (1968).

[8]H. R. Weller, Phys. Letters 30B, 409 (1969).

[9]P. N. Shrivastava, F. Boreli, and B. B. Kinsey, Phys. Rev. 169, 842 (1968).

[10]Targets were prepared by J. L. Duggan of Oak Ridge National Laboratory.

[11]R. L. Taschek and A. Hemmendinger, Phys. Rev. 74, 373 (1948).

[12]The program MULTI was written by D. L. Sellin of Duke University.

[13]A. M. Lane and R. G. Thomas, Rev. Mod. Phys. 30, 257 (1958).

[14]J. M. Blatt and L. C. Biedenharn, Rev. Mod. Phys. 24, 258 (1952).

[15]J. J. Ramirez, H. R. Weller, and R. A. Blue, Phys. Letters 32B, 361 (1970).

[16]H. M. Kuan, private communication.

[17]K. H. Bhatt, Nucl. Phys. 39, 375 (1962).

[18]R. J. DeMeijer, H. F. J. Van Royen, and P. J. Brussard, Nucl. Phys. A164, 64 (1969).

[19]H. R. Weller and H. A. Van Rinsvelt, Nucl. Phys. A129, 64 (1969).

[20]R. F. Jackson and H. R. Weller, Nucl. Phys. A160, 247 (1971).

[21]J. S. Lopes, O. Häusser, J. J. Rose, A. R. Poletti, and M. F. Thomas, Nucl. Phys. 76, 223 (1966).

Two-Body Interactions: The Method of Correlated Quasiparticles. I.

R. R. Chasman

Chemistry Division, Argonne National Laboratory, Argonne, Illinois 60439

(Received 27 September 1971)

A method is proposed for determining the ground state of the Hamiltonian

$$H = \sum_k \epsilon_k N_k - \sum_{ijkl} V_{ijkl} a_i^\dagger a_j^\dagger a_k a_l$$

when the residual interaction is such that

$$\langle a_i^\dagger a_j^\dagger a_k a_l \rangle = \langle N_i N_j (1 - N_k)(1 - N_l) \rangle^{1/2} \langle N_k N_l (1 - N_i)(1 - N_j) \rangle^{1/2}$$

is a good approximation. The method is applied to pairing interactions involving one type of nucleon as well as to the generalized pairing problem containing neutron-neutron, neutron-proton, and proton-proton interactions.

I. INTRODUCTION

In this work, we study the ground state of the Hamiltonian

$$H = \sum_k \epsilon_k N_k - \sum_{ijkl} V_{ijkl} a_i^\dagger a_j^\dagger a_k a_l \qquad (1)$$

when the following approximation is valid for the ground-state wave function:

$$\langle a_i^\dagger a_j^\dagger a_k a_l \rangle = \langle N_i N_j (1 - N_k)(1 - N_l) \rangle^{1/2}$$
$$\times \langle N_k N_l (1 - N_i)(1 - N_j) \rangle^{1/2} . \qquad (2)$$

The symbol $a_i^\dagger$ (a_i) denotes a fermion creation (annihilation) operator; N_i denotes a number operator; and the angular brackets enclose ground-state expectation values. In Sec. II, we discuss the conditions under which Eq. (2) is a reasonable approximation and consider the implications of Eq. (2) with respect to particle correlations. In Sec. III, we make a detailed study of particle correlations in the case of the pairing-force model,

and use this approach to construct ground-state solutions of the simple pairing model. These solutions are compared with exact solutions of the pairing Hamiltonian. The same approach is applied to the generalized pairing problem which includes proton-proton, proton-neutron, and neutron-neutron pairing interactions. The correlations in the ground-state wave function of this problem are analyzed in detail. Our hope is to apply this approach to other two-body interactions in future publications.

II. GENERAL CONSIDERATIONS

The ground-state (or any other state) wave function is of the form:

$$|\Psi\rangle = \sum_{i>j>k>l\cdots} C_{ijkl\ldots} a_i^\dagger a_j^\dagger a_k^\dagger a_l^\dagger \cdots |0\rangle , \qquad (3)$$

where $|0\rangle$ denotes the true vacuum state, and $C_{ijkl\ldots}$ denotes the amplitudes of the various configurations in the ground-state wave function. In terms of the coefficients $C_{ijkl\ldots}$, the approxima-